ISSN: 2229-7359 Vol. 11 No. 25s,2025

https://theaspd.com/index.php

# Wet Chemically Synthesized Optical Investigation Of Tb<sup>3+</sup>/Eu<sup>3+</sup> Activated/Co-Activated Batio<sub>3</sub> Phosphors By Energy Transfer Mechanism

# Avinash V. Bharati<sup>1\*</sup>, Shreya Bharati<sup>2</sup>

- <sup>1</sup> Department of Chemistry, Ramdeobaba College of Engineering and Management, Nagpur, India
- <sup>2</sup> Department of Information Technology, Monash University, Clayton Campus, Melbourne, Australia
- \*Corresponding author: bharatiav@rknec.edu

Abstract: In recent years, rare-earth-doped inorganic phosphors have gained significant attention in the field of display technologies. In this study, BaTiO<sub>3</sub> phosphors doped and co-doped with Tb<sup>3+</sup> and Eu<sup>3+</sup> ions were synthesized using the wet chemical method. The crystal structure and phase composition of the obtained phosphors were characterized through X-ray diffraction (XRD) combined with Rietveld refinement. Surface morphology and elemental composition were investigated using scanning electron microscopy (SEM) along with elemental analysis. Photoluminescence (PL) studies revealed that, under excitations at 265 nm, 395 nm, and 465 nm, Eu<sup>3+</sup>doped and Tb<sup>3+</sup>/Eu<sup>3+</sup> co-doped BaTiO<sub>3</sub> phosphors displayed prominent emissions: an orange peak at 595 nm and a red peak at 614 nm corresponding to the  ${}^5\!D_0 \rightarrow {}^7\!F_1$  and  ${}^5\!D_0 \rightarrow {}^7\!F_2$  transitions of Eu<sup>3+</sup>, respectively, while Tb<sup>3+</sup>doping yielded green emission. Upon satisfying the spectral overlap condition, co-doping both ions in the host matrix resulted in photoluminescence with color tunability from green to red. These findings suggest that the synthesized phosphors are promising candidates for white light-emitting diodes (WLEDs) and display device applications.

Keywords: Wet Chemical; Lamp Phosphor; White Light-Emitting Diodes; Color Tunability; Energy Transfer

### 1. INTRODUCTION

Because of its many uses, including as capacitors, electro optical systems, pyroelectric infrared sensors, ultrasonic transducers, positive temperature coefficient (PTC) resistors, and more, barium titanate (BaTiO<sub>3</sub>) is being explored in great detail[1,2]. By utilising diverse preparation techniques and dopants, BaTiO<sub>3</sub>'s electrical characteristics can be modified. The luminescence properties of BaTiO<sub>3</sub> nanopowders generated by different processes may also be significantly influenced by the varied types of defects that have been found. Among the chemical elements utilized as dopants for BaTiO<sub>3</sub> are rare earths[3-6]. One of these, lanthanum, is a donor dopant that fills the Ba sites in the BaTiO<sub>3</sub> crystal lattice. When barium titanate (BaTiO<sub>3</sub>) is doped with RE, it exhibits a shift in electrical resistance, particle size, and symmetry from tetragonal to cubic [7–9]. The BaTiO<sub>3</sub> structure becomes defective due to RE-doping, as it results in alterations to the A and B sites as well as an A-site vacancy. It follows that doping should have an impact on optical properties. It was demonstrated that the optical band gap value (derived from UV-Vis spectra) for RE-doped BaTiO<sub>3</sub> samples synthesised by solid state reaction reduced as La concentration increased. On doped samples, however, no broadening or shifting of the luminescence peaks is seen. However, it is known that the process of synthesis, which can result in the production of more or less structural flaws, might affect the physical properties (namely luminescence). There were several techniques utilised to prepare RE<sup>3+</sup> doped BaTiO<sub>3</sub>, including coprecipitation, spray pyrolysis, sol-gel, solid state reaction, Pechini method, etc[7,10-15]. We want to investigate the effects of rare earth doping on luminescence spectra.

Rare earth ion luminescence in solids has previously been observed in recent decades[16–19]. Due to the unique electrical arrangement of rare earth elements, rare earth luminescent materials have numerous emission spectra due to the rich energy level structure of their 4f orbit. Rare earth polychromatic luminescence materials have drawn increasing attention in recent years from those working in the fields of displays, lighting, lasers, and photoelectric devices[20–23]. Tb<sup>3+</sup> is a superior ion for activating green lights. In BaTiO<sub>3</sub> phosphors, the energy can move from Tb<sup>3+</sup> to Eu<sup>3+</sup>, and it may also enhance the luminous characteristics of Eu<sup>3+</sup> doped BaTiO<sub>3</sub> phosphors[10,24]. If different ratios of Eu<sup>3+</sup> and Tb<sup>3+</sup> are doped, the emission colour of the co-doped Eu<sup>3+</sup>, Tb<sup>3+</sup> BaTiO<sub>3</sub> phosphors can shift from green to red. The kind of phosphors was mentioned as having promise for use as materials in anti-counterfeiting systems. Analyzing the colour and intensity changes in Tb<sup>3+</sup> and Eu<sup>3+</sup> co-doped BaTiO<sub>3</sub> phosphors is particularly helpful in

ISSN: 2229-7359 Vol. 11 No. 25s,2025

https://theaspd.com/index.php

elucidating the physical process underlying the energy transfer from Tb<sup>3+</sup> to Eu<sup>3+</sup> in the phosphors. In light of the aforementioned, we created Tb<sup>3+</sup> and Eu<sup>3+</sup> co-doped BaTiO<sub>3</sub> micro-crystals in our work using the precipitation method. We looked at the simples' X-ray diffraction spectra and scanning electron microscopy pictures. PL investigations have been conducted in Tb<sup>3+</sup> and Eu<sup>3+</sup> phosphor to confirm luminous characteristics and analyze energy transmission[25–27].

#### 2. Synthesis and Characterizations

BaTiO<sub>3</sub> phosphor powders, singly doped and co-doped with Tb³+ and Eu³+ ions, were synthesized via a wet chemical route, followed by annealing in a reducing atmosphere. In the preparation process, stoichiometric quantities of Ba(NO<sub>3</sub>)<sub>2</sub>·4H<sub>2</sub>O and TiO<sub>2</sub> were thoroughly mixed. High-purity Eu<sub>2</sub>O<sub>3</sub> (99.99%) and Tb<sub>4</sub>O<sub>7</sub> (99.99%) were converted into respective nitrate by dissolving in minimum amount of nitric acid, which were then mixed in a small volume of double-distilled water. The solution was continuously stirred and heated in a water bath at 85 °C to obtain a homogeneous precipitate. This precipitate was dried overnight in a hot-air oven, after which the dried mass was collected, ground for 5 minutes, and subsequently used for further characterization.

The phase purity of the prepared BaTiO<sub>3</sub> phosphor was examined using multiple characterization techniques. Powder X-ray diffraction (XRD) patterns were recorded with Cu K $\alpha$  radiation ( $\lambda$  = 1.5405 Å) on a RIGAKU MiniFlex 600 diffractometer for structural analysis. Fourier transform infrared spectroscopy (FTIR) was employed to study the vibrational modes of the sample. Additionally, photoluminescence (PL) studies, including both excitation and emission spectra, were performed using a SHIMADZU RF-5301 spectrofluorophotometer to explore the optical properties.

## 3. RESULT AND DISCUSSION

# A. XRD Analysis

Step scanning at intervals of 0.02° was used to monitor the XRD pattern of the synthesized Ba<sub>1xy</sub>TiO<sub>3</sub>:xTb<sup>3+</sup>; yEu<sup>3+</sup> phosphors in the range of (20–80)°, as shown in Figure 1. The detected diffraction peaks are in good agreement with JCPDS card number 82-1175. The peaks are thin, clear, and distinct, suggesting that the diffraction pattern is clearly indexed. The existence of these peaks is explained by the possibility that rare earth ions, whose ionic radii are similar to those of Ba<sup>2+</sup>, will occupy these interstitial positions. The near ionic radius match between Ba<sup>2+</sup> ions and rare earths explains this substitution. But because of the discrepancy in ionic radii, the Ti<sup>4+</sup> sites whose ionic radius is remained unsubstituted, which explains why they are absent from the substitution process. It is possible that both phases are present in the sample because trace amounts of BaTi<sub>2</sub>O<sub>5</sub> have been observed to peak with BaTiO<sub>3</sub> in the XRD pattern. Depending on the relative prevalence of these two phases within the material, a correlation between them may show up as a change in peak intensities. The distinctive peaks of BaTiO<sub>3</sub> will show up more clearly and intensely in the XRD pattern when it is the dominant phase. Because of its reduced presence in these circumstances, the intensity of BaTi<sub>2</sub>O<sub>5</sub> peaks will be relatively lower. On the other hand, if BaTi<sub>2</sub>O<sub>5</sub> takes over as the predominant phase, its distinctive peaks will stand out more and have higher intensities in the XRD pattern. Thereafter, the BaTiO<sub>3</sub> peaks would become less visible and intense, suggesting that there was less BaTiO<sub>3</sub> in the sample overall. The observed XRD pattern may be influenced by the correlation between these phases' dominance. The concentrations of each phase's peaks within the sample are directly correlated with their intensities. When one phase predominates, its distinctive peaks stand out more, and when the other phase is less prevalent, the strength of its peaks diminishes.

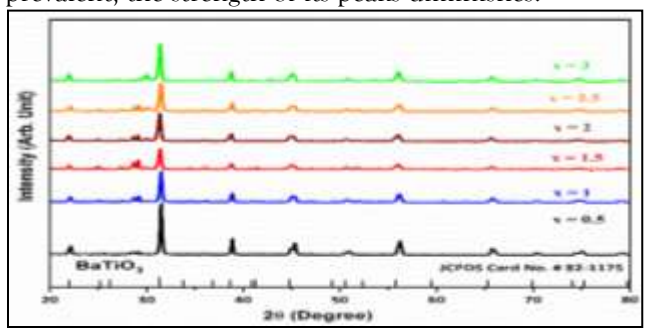


Figure 1: XRD analysis of Ba<sub>1-xy</sub>TiO<sub>3</sub>:xTb<sup>3+</sup>, yEu<sup>3+</sup> phosphors.

ISSN: 2229-7359 Vol. 11 No. 25s,2025

https://theaspd.com/index.php

### **B.** FTIR Analysis

The BaTiO<sub>3</sub> perovskite phosphor's FT-IR illustrations are displayed in Figure 2. The common explanation for the band at 1421 cm<sup>-1</sup> is the asymmetric stretching vibration of carbonate groups. The carbonate groups' symmetric stretching vibration is correlated with the absorption at 1003 cm<sup>-1</sup>. This peak provides additional evidence that carbonate ions are present in the sample. The carbonate group's out-of-plane bending vibration is linked to the band at 696 cm<sup>-1</sup>. The recognition of carbonate ions in the material is also supported by this vibration mode. The presence of the Ti-O stretching vibration band at 553 cm<sup>-1</sup> in the FT-IR spectra, which is compatible with the findings from other analytical techniques like XRD, strongly supports the establishment of the perovskite structure in the prepared material. The effective synthesis of the desired perovskite phase is confirmed by this validation. The characteristic Ti-O stretching vibrations in the infrared spectra of BaTiO<sub>3</sub> are well-known. The absorption peak located at 560 cm<sup>-1</sup> is indicative of the particular vibration mode of the Ti-O bonds seen in the BaTiO<sub>3</sub> structure. In the FT-IR spectra, the absorption bands at wave numbers (723 and 772) cm<sup>-1</sup> are linked to metal-oxygen (M-O) vibrations, specifically with the bonds between titanium and oxygen (Ti-O) and titanium and oxygen-titanium (Ti-O-Ti)[3,28-30].

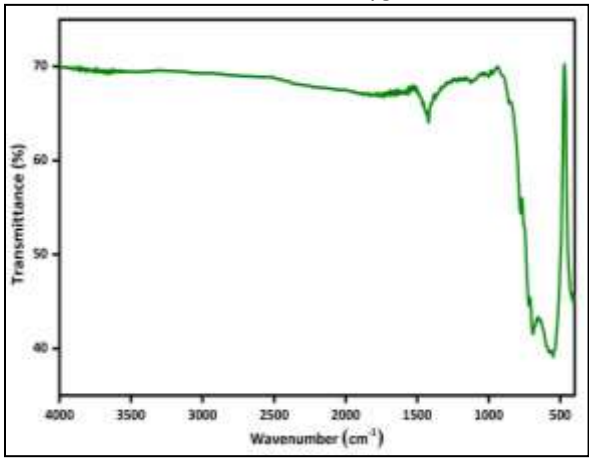


Figure 2: FTIR analysis of BaTiO<sub>3</sub> phosphor.

# C. Photoluminescence Investigation

On doping  $Tb^{3+}$  ions, PL emission and excitation spectra were observed for the identical host lattice. Four peaks in the NUV region are visible in the PL excitation spectra, with peak positions at 351 nm, 368 nm, and 377 nm. The  ${}^{7}F_{6} \rightarrow {}^{5}L_{9}$  transitions are responsible for the peaks at 351 and 368 nm, whereas the  ${}^{7}F_{6} \rightarrow {}^{5}D_{3}$  transition shown in Figure 3 is responsible for the peak at 377 nm[31]. The two wavelengths at which the peaks at 351 and 377 nm are the most influential are those at which we record PL emission spectra. Two strong emission peaks were found at 452 and 545 nm, along with a few smaller, more broadly orientated peaks at 452 and 488 the wavelengths. Figures 4 and 5 show the peaks at 452 and 488 nm, which are caused by  ${}^{5}D_{4} \rightarrow {}^{5}F_{6}$  and 544 nm, which are caused by  ${}^{5}D_{4} \rightarrow {}^{5}F_{5}$  transitions[32–34].

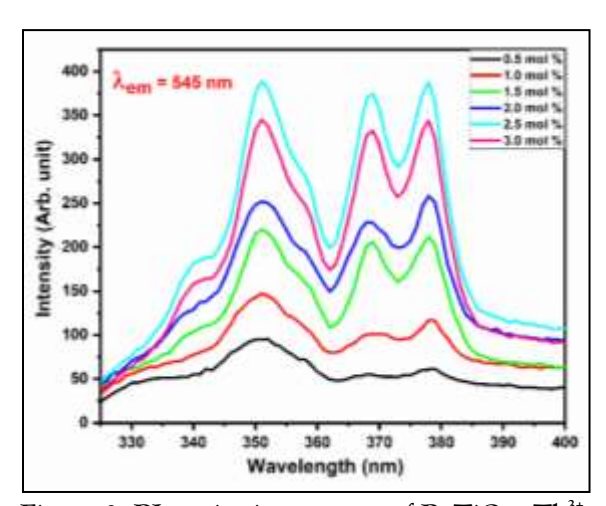


Figure 3: PL excitation spectra of BaTiO<sub>3</sub>:xTb<sup>3+</sup> phosphor monitored at emission of 545 nm.

ISSN: 2229-7359 Vol. 11 No. 25s,2025

https://theaspd.com/index.php

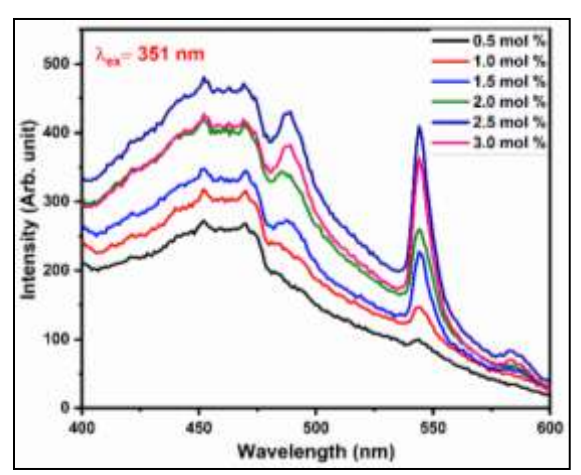


Figure 4: PL emission spectra of BaTiO<sub>3</sub>:xTb<sup>3+</sup> phosphor at excitation of 351 nm.

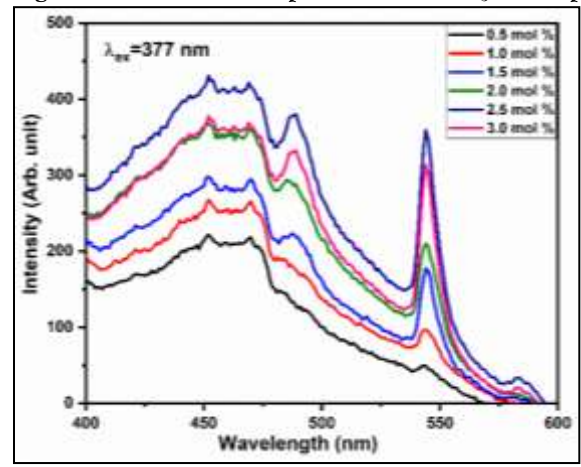


Figure 5: PL emission spectra of BaTiO<sub>3</sub>:xTb<sup>3+</sup> phosphor at excitation of 377 nm.

The PL excitation spectra of BaTiO<sub>3</sub>: x Eu<sup>3+</sup> phosphors, as illustrated in Figure 6, exhibit two distinct excitation peaks at 394 nm and 466 nm. These peaks, recorded using an emission wavelength of 594 nm, correspond to the  $^7F_0 \rightarrow ^5L_6$  and  $^7F_0 \rightarrow ^5D_2$  electronic transitions of Eu<sup>3+</sup> ions[35-40], correspondingly. When excited at wavelengths of 394 nm and 466 nm, as illustrated in Figures 7 and 8, the phosphor exhibits two prominent emission peaks positioned at 594 nm and 614 nm. These emissions are associated with the  $^5D_0 \rightarrow ^7F_1$  magnetic dipole transition and the  $^5D_0 \rightarrow ^7F_2$  electric dipole transition of Eu<sup>3+</sup> ions, respectively[41].

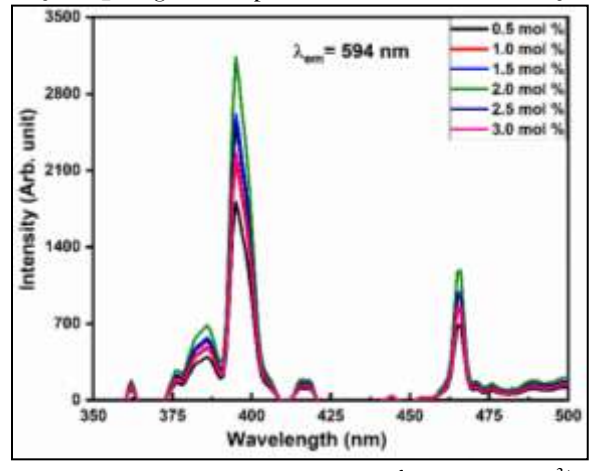


Figure 6: PL excitation spectra of BaTiO<sub>3</sub>:xEu<sup>3+</sup> phosphor monitored at emission of 594 nm.

ISSN: 2229-7359 Vol. 11 No. 25s,2025

https://theaspd.com/index.php

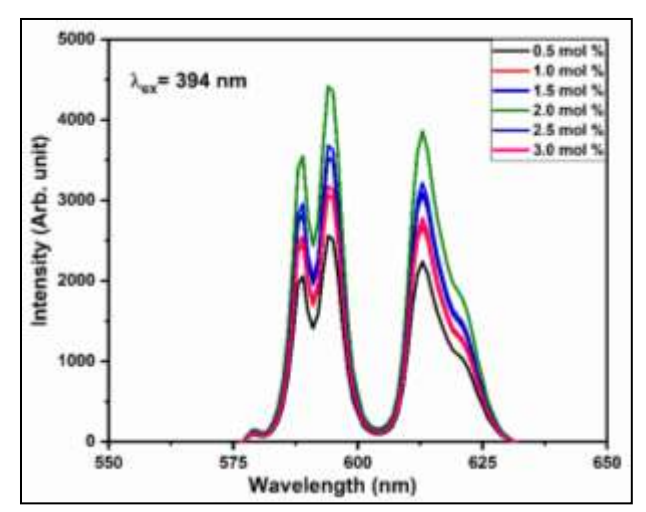


Figure 7: PL emission spectra of BaTiO<sub>3</sub>:xEu<sup>3+</sup> phosphor at excitation of 394 nm.

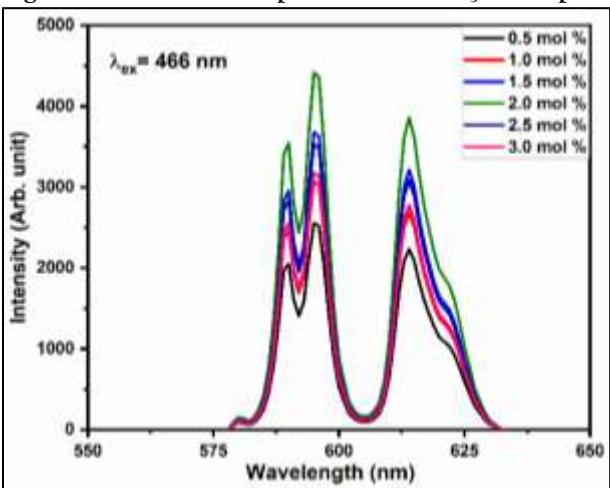


Figure 8: PL emission spectra of BaTiO<sub>3</sub>:xEu<sup>3+</sup> phosphor at excitation of 466 nm.

In BaTiO<sub>3</sub> phosphors doped with Tb³+ and Eu³+, the emission intensity increases with dopant concentration up to about 2.5 mol% for Tb³+ and 2 mol% for Eu³+, after which it declines. This reduction is attributed to the concentration quenching phenomenon. Such quenching occurs due to the critical transfer distance (Rc), defined as the separation between a host ligand and an activator ion at the critical concentration (Xc). The magnitude of Rc determines the type of interaction responsible for quenching. When Rc is less than 5 Å, exchange interactions dominate the reduction in intensity, whereas for values greater than 5 Å, multipolar interactions are primarily responsible. Critical transfer distance is determined by the Blasse theory[18];

$$R_{\rm C} = 2 \left(\frac{3V}{4 \prod X_{\rm C} N}\right)^{1/3} \tag{1}$$

Here if V= 196.90 Å<sup>3</sup> is the volume of the unit cell,  $X_c = 2.5$  and 2 mol % for  $Tb^{3+}$  and  $Eu^{3+}$  respectively are the optimal concentration, N=2 is the number of cations in the unit cell. Now according to formula,  $R_C$  is 4.22 and 4.54 for both  $Tb^{3+}$  and  $Eu^{3+}$  ions respectively. Therefore, exchange interaction is accountable for the concentration quenching effect in  $Tb^{3+}$ ,  $Eu^{3+}$  doped  $BaTiO_3$  phosphors.

Dexter theory was applied to obtain more precise information regarding the interactions accountable for the concentration quenching in  $Tb^{3+}$  and  $Eu^{3+}$  doped  $BaTiO_3$  phosphors[37,42];

$$\frac{I}{x} = k[1 + \beta. x^{\frac{\theta}{3}}]^{-1}$$
 (2)

The emission intensity of the rare-earth-activated phosphor is represented here, where x indicates the doping concentration, and k and  $\beta$  are constants. According to Van Uitert's theory, as discussed in previous literature, the nature of the interaction causing concentration quenching is determined by the value of  $\theta[43]$ . Relation between log (x) and log (I/x) are depicted in Figure 9 and 10 for Tb<sup>3+</sup> doped BaTiO<sub>3</sub> and Eu<sup>3+</sup> doped BaTiO<sub>3</sub> phosphors respectively[44–46]. Slope of given linear fits for the Tb<sup>3+</sup> doped BaTiO<sub>3</sub> and Eu<sup>3+</sup> doped

ISSN: 2229-7359 Vol. 11 No. 25s,2025

https://theaspd.com/index.php

BaTiO<sub>3</sub> phosphors are -0.0389 and -1.0462 respectively. Therefore, values of  $\theta$  are 0.1167 and 3.1386 for Tb<sup>3+</sup> and Eu<sup>3+</sup> respectively which are nearly equal to 3 therefore exchange interaction is responsible for the concentration quenching for both the rare earth ions.

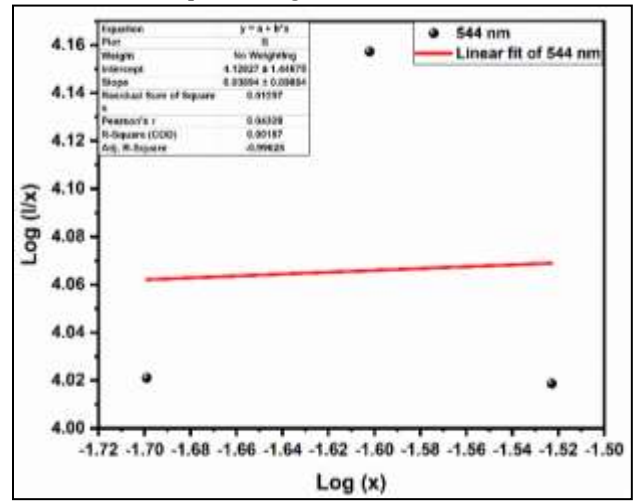


Figure 9: Log(x) Vs Log(I/x) for Tb<sup>3+</sup> doped BaTiO<sub>3</sub> phosphors.

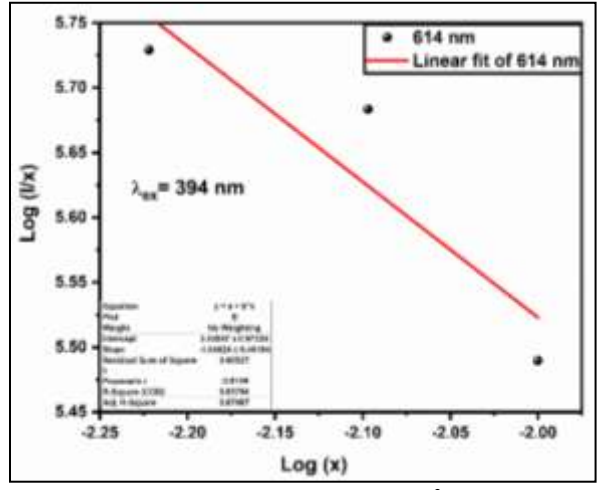


Figure 10: Log(x) Vs Log(I/x) for Eu<sup>3+</sup> doped BaTiO<sub>3</sub> phosphors.

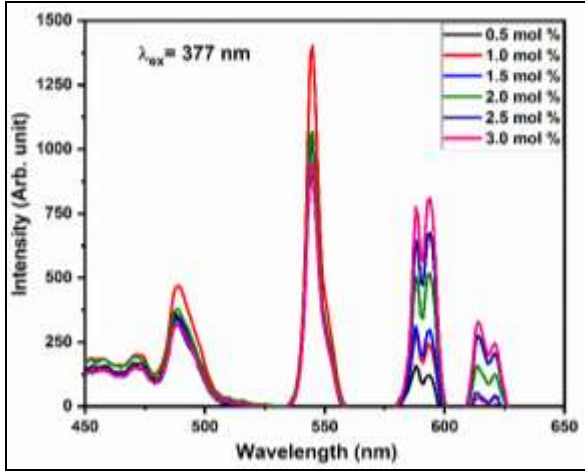


Figure 11: PL emission spectra of 2.5 mol % Tb<sup>3+</sup>, x mol % Eu<sup>3+</sup> activated BaTiO<sub>3</sub> phosphors.

The energy transfer from  $Tb^{3+}$  to  $Eu^{3+}$  has taken place as a result of the BaTiO<sub>3</sub> phosphors'  $Tb^{3+}$  and  $Eu^{3+}$  ions meeting the spectral overlapping conditions of excitation-excitation overlapping[36]. Figure 11 presents the emission spectra of  $Tb^{3+}/Eu^{3+}$  co-doped NaLa(MoO<sub>4</sub>)<sub>2</sub> phosphor monitored at 545 nm under 377 nm excitation. The spectra exhibit three characteristic emission peaks: a green emission at 545 nm from the  $^5D_4$   $\rightarrow$   $^7F_5$  transition of  $Tb^{3+}$ , and orange-red emissions at 594 nm ( $^5D_0 \rightarrow$   $^7F_1$ ) and 614 nm ( $^5D_0 \rightarrow$   $^7F_2$ ) from

ISSN: 2229-7359 Vol. 11 No. 25s,2025

https://theaspd.com/index.php

Eu<sup>3+</sup>. A progressive decrease in the 545 nm emission intensity with increasing Eu<sup>3+</sup> concentration, accompanied by an enhancement of Eu<sup>3+</sup> emissions, indicates efficient Tb<sup>3+</sup>  $\rightarrow$  Eu<sup>3+</sup> energy transfer. The corresponding energy transfer mechanism is illustrated in Figure 12.

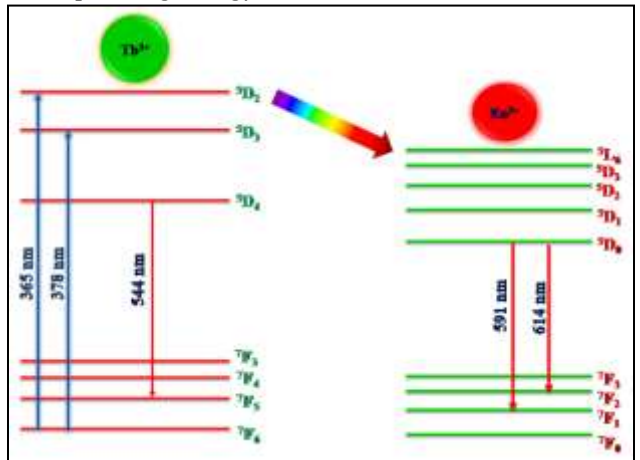


Figure 12: Energy transfer mechanism of Tb<sup>3+</sup> to Eu<sup>3+</sup> energy transfer. (Reproduced with the permission from the ref.[27] © RSC Publications 2023)

#### D. CIE Photochromaticity

The chromaticity coordinates of the Tb³+, Eu³+ activated/co-activated BaTiO₃ phosphor were determined by the Commission de I Eclairage (CIE) and can be seen in Figure 13[42]. The chromatic coordinates of BaTiO₃ phosphors co-doped with Tb³+ and Eu³+ are listed in Table 1. As depicted in Figure 13, these phosphors emit white light. With the gradual increase in Eu³+ concentration, the coordinates of BaTiO₃:Tb³+, Eu³+ phosphors shift closer to the white light region, demonstrating their tunable emission properties. The variation in dopant concentration, as shown in Table 1, also influences the color purity of the phosphors, which can be evaluated using the given formula.[42,46–50];

Colorpurity = 
$$\frac{\sqrt{(X-X_i)^2 + (Y-Y_i)^2}}{\sqrt{(X_d-X_i)^2 + (Y_d-Y_i)^2}} * 100 \%$$
 (4)

TABLE I. Summary of CIE color co-ordinates and other parameters of BaTiO<sub>3</sub>:Tb<sup>3+</sup>, Eu<sup>3+</sup> co-activated phosphor:

Sr No.	Sample	X	Y	$X_d$	$Y_d$	Color Purity (%)
1.	BaTiO <sub>3</sub> : 2.5 mol % Tb <sup>3+</sup> , 0.5	0.2059	0.2796	0.2686	0.7178	61.16
	mol % Eu <sup>3+</sup>					
2.	BaTiO <sub>3</sub> : 2.5 mol % Tb <sup>3+</sup> , 1	0.2245	0.3000	0.2686	0.7178	51.57
	mol % Eu <sup>3+</sup>					
3.	BaTiO <sub>3</sub> : 2.5 mol % Tb <sup>3+</sup> , 1.5	0.2442	0.2974	0.2686	0.7178	42.39
	mol % Eu <sup>3+</sup>					
4.	BaTiO <sub>3</sub> : 2.5 mol % Tb <sup>3+</sup> , 2	0.2734	0.2895	0.2686	0.7178	28.94
	mol % Eu <sup>3+</sup>					
5.	BaTiO <sub>3</sub> : 2.5 mol % Tb <sup>3+</sup> , 2.5	0.3216	0.3067	0.2686	0.7178	5.69
	mol % Eu <sup>3+</sup>					
6.	BaTiO <sub>3</sub> : 2.5 mol % Tb <sup>3+</sup> , 3	0.3398	0.3165	0.2686	0.7178	3.32
	mol % Eu <sup>3+</sup>					

ISSN: 2229-7359 Vol. 11 No. 25s,2025

https://theaspd.com/index.php

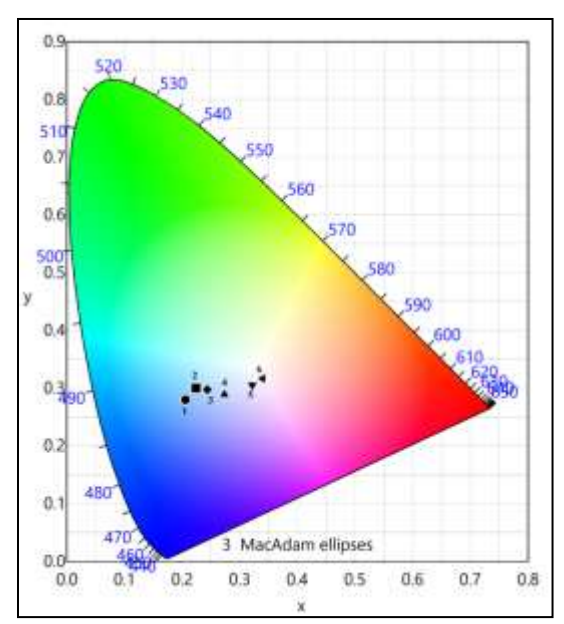


Figure 13: CIE chromaticity of 2.5 mol % Tb<sup>3+</sup> x mol % Eu<sup>3+</sup> activated BaTiO<sub>3</sub> phosphors.

#### 4. CONCLUSION

In this study, Tb³+ and Eu³+ doped/co-doped BaTiO₃ phosphors were prepared using the sol-gel technique to investigate their charge compensation behavior and photochromic properties. Various analytical methods were employed to confirm the structural and optical features of the synthesized phosphors. X-ray diffraction (XRD) confirmed their crystalline structure, while Fourier-transform infrared (FTIR) spectroscopy identified their vibrational modes. Optical studies revealed a tunable emission color ranging from blue to white, with the CIE chromaticity coordinates showing a shift dependent on Eu³+ ion concentration. These results indicate that the phosphor serves as a promising photochromic blue-to-white emitter, suitable for white light-emitting diodes (WLEDs) and display technologies.

#### REFERENCES

- D.S. Smith, N. Ghayoub, I. Charissou, O. Bellon, P. Abélard, A.H. Edwards, Transient thermal gradients in barium titanate Positive Temperature Coefficient (PTC) thermistors, J. Am. Ceram. Soc. 81 (1998) 1789–1796. https://doi.org/10.1111/j.1151-2916.1998.tb02549.x.
- J. Liu, S. Gong, L. Quan, B. Chen, D. Zhou, Reoxidation effects of Ba-excessive barium titanate ceramics for laminated positive temperature coefficient thermistors, J. Am. Ceram. Soc. 95 (2012) 1640–1644. https://doi.org/10.1111/j.1551-2916.2011.05041.x.
- A.E. Souza, S.R. Teixeira, C.M. -Santos, W.H. Schreiner, P.N. Lisboa Filho, E. Longo, Photoluminescence activity of Ba<sub>1-x</sub>Ca<sub>x</sub>TiO<sub>3</sub>: Dependence on particle size and morphology, J. Mater. Chem. C 2 (2014) 7056–7070. https://doi.org/10.1039/c4tc00897a.
- A.C. Ianculescu, C.A. Vasilescu, M. Crisan, M. Raileanu, B.S. Vasile, M. Calugaru, D. Crisan, N. Dragan, L. Curecheriu, L. Mitoseriu, Formation mechanism and characteristics of lanthanum-doped BaTiO<sub>3</sub> powders and ceramics prepared by the sol-gel process, Mater. Charact. 106 (2015) 195–207. https://doi.org/10.1016/j.matchar.2015.05.022.
- ➤ S. Fuentes, R. Espinoza-González, M. Rosales, J. León, Effects of Eu³\* on the morphological, structural and optical properties of BaTiO₃@ZnO:Eu nanoparticles, J. Alloys Compd. 846 (2020) 156452. https://doi.org/10.1016/j.jallcom.2020.156452.
- o Patra, C.S. Friend, R. Kapoor, P.N. Prasad, Fluorescence upconversion properties of Er³\*-doped TiO<sub>2</sub> and BaTiO<sub>3</sub> nanocrystallites, Chem. Mater. 15 (2003) 3650–3655. https://doi.org/10.1021/cm020897u.
- Rached, M.A. Wederni, K. Khirouni, S. Alaya, R.J. Martín-Palma, J. Dhahri, Structural, optical and electrical properties of barium titanate, Mater. Chem. Phys. 267 (2021) 124600. https://doi.org/10.1016/j.matchemphys.2021.124600.
- M. Borah, D. Mohanta, Effect of Gd<sup>3+</sup> doping on structural, optical and frequency-dependent dielectric response properties of pseudo-cubic BaTiO<sub>3</sub> nanostructures, Appl. Phys. A Mater. Sci. Process. 115 (2014) 1057–1067. https://doi.org/10.1007/s00339-013-7941-7.
- M. Cernea, M. Secu, R. Radu, P. Ganea, V.A. Surdu, R. Trusca, E.T. Vasile, E.C. Secu, Structural, electrical properties and photoluminescence analyses of the terbium doped barium titanate, J. Alloys Compd. 878 (2021) 160380. https://doi.org/10.1016/j.jallcom.2021.160380.
- W. Li, Z. Xu, R. Chu, P. Fu, J. Hao, Structure and electrical properties of BaTiO<sub>3</sub> prepared by sol-gel process, J. Alloys Compd. 482 (2009) 137-140. https://doi.org/10.1016/j.jallcom.2009.02.137.

ISSN: 2229-7359 Vol. 11 No. 25s,2025

https://theaspd.com/index.php

o Zhu, Q. Zhao, Z. Cai, L. Guo, L. Li, X. Wang, High reliable non-reducible ultra-fine BaTiO<sub>3</sub>-based ceramics fabricated via solid-state method, J. Alloys Compd. 829 (2020) 154496. https://doi.org/10.1016/j.jallcom.2020.154496.

- H. Jena, K.V.G. Kutty, T.R.N. Kutty, Proton transport and structural relations in hydroxyl-bearing BaTiO<sub>3</sub> and its doped compositions synthesised by wet-chemical methods, Mater. Res. Bull. 39 (2004) 489–511. https://doi.org/10.1016/j.materresbull.2003.10.004.
- S.K. Lee, T.J. Park, G.J. Choi, K.K. Koo, S.W. Kim, Effects of KOH/BaTi and Ba/Ti ratios on synthesis of BaTiO<sub>3</sub> powder by coprecipitation/hydrothermal reaction, Mater. Chem. Phys. 82 (2003) 742–749. https://doi.org/10.1016/j.matchemphys.2003.07.003.
- V. Sebastian, Design of Magnetostrictive Nanoparticles for Magnetoelectric Composites, Magnetoelectric Polym. Compos. (2017) 125–151. https://doi.org/10.1002/9783527801336.ch5.
- B.D. Stojanovic, A.S. Dzunuzovic, N.I. Ilic, Review of methods for the preparation of magnetic metal oxides, Elsevier Inc., 2018. https://doi.org/10.1016/B978-0-12-811180-2.00017-7.
- S.R. Bhelave, A.R. Kadam, A.N. Yerpude, S.J. Dhoble, Intensity enhancement of photoluminescence in Tb<sup>3+</sup>/Eu<sup>3+</sup> co-doped Ca<sub>14</sub>Zn<sub>6</sub>Al<sub>10</sub>O<sub>35</sub> phosphor for WLEDs, Luminescence (2023) 379–388. https://doi.org/10.1002/bio.4456.
- ➤ R. V Tikale, A.R. Kadam, S.J. Dhoble, Synthesis and luminescence properties of Bi<sup>3+</sup> activated Ba<sub>3</sub>WO<sub>5</sub>Cl<sub>2</sub> phosphors for plant cultivation applications, Chem. Data Collect. 40 (2022) 100891. https://doi.org/10.1016/j.cdc.2022.100891.
- ▶ R.G. Deshmukh, A.R. Kadam, S.J. Dhoble, Energy transfer mechanism in K₂Ba(PO₄)F:Dy³\*, Eu³\* co-activated phosphor: Spectral tuning phosphor for photovoltaic efficiency enhancement, J. Mol. Struct. 1257 (2022) 132603. https://doi.org/10.1016/j.molstruc.2022.132603.
- ➤ P.N. Parale, A.R. Kadam, K. V. Dabre, S.J. Dhoble, Spectroscopic investigation of KBa₂(PO₃)₅:Mn⁴⁺ activated glasses for plant cultivation applications, Mater. Lett. X 18 (2023) 100191. https://doi.org/10.1016/j.mlblux.2023.100191.
- S. Som, P. Mitra, V. Kumar, V. Kumar, J.J. Terblans, H.C. Swart, S.K. Sharma, The energy transfer phenomena and colour tunability in Y<sub>2</sub>O<sub>2</sub>S:Eu<sup>3+</sup>/Dy<sup>3+</sup> micro-fibers for white emission in solid state lighting applications, Dalt. Trans. 43 (2014) 9860–9871. https://doi.org/10.1039/c4dt00349g.
- G. Gu, W. Xiang, C. Yang, X. Liang, Synthesis and luminescence properties of a H<sub>2</sub> annealed Mn-doped Y<sub>3</sub>Al<sub>5</sub>O<sub>12</sub>:Ce<sup>3+</sup> single crystal for WLEDs, CrystEngComm 17 (2015) 4554–4561. https://doi.org/10.1039/c5ce00641d.
- X. yuan Sun, S. ming Huang, X. san Gong, Q. chun Gao, Z. piao Ye, C. yan Cao, Spectroscopic properties and simulation of white-light in Dy<sup>3+</sup>-doped silicate glass, J. Non. Cryst. Solids 356 (2010) 98–101. https://doi.org/10.1016/j.jnoncrysol.2009.10.009.
- Y. V. Baklanova, L.G. Maksimova, O.A. Lipina, A.P. Tyutyunnik, V.G. Zubkov, Novel orange-red-emitting Li<sub>5+x</sub>Ca<sub>x</sub>La<sub>3-x</sub>Ta<sub>2</sub>O<sub>12</sub>:Sm<sup>3+</sup> (x = 0; 1) phosphors: Crystal structure, luminescence and thermal quenching studies, J. Lumin. 224 (2020) 117315. https://doi.org/10.1016/j.jlumin.2020.117315.
- Kumari, V.K. Rai, K. Kumar, Yellow-orange upconversion emission in Eu<sup>3+</sup>-Yb<sup>3+</sup> codoped BaTiO<sub>3</sub> phosphor, Spectrochim. Acta Part A Mol. Biomol. Spectrosc. 127 (2014) 98-101. https://doi.org/10.1016/j.saa.2014.02.023.
- X. Liu, X. Chen, Y. Yu, W. Xie, Y. Zhao, S. Luo, G. Mei, J. Lin, Broad-band excited and tunable luminescence of CaTbAl<sub>3</sub>O<sub>7</sub>:Re<sup>3+</sup> (Re<sup>3+</sup> = Ce<sup>3+</sup> and/or Eu<sup>3+</sup>) nanocrystalline phosphors for near-UV wleds, Inorg. Chem. 59 (2020) 12348–12361.
- https://doi.org/10.1021/acs.inorgchem.0c01440.
- A.U. Trápala-Ramírez, J.L.N. Gálvez-Sandoval, A. Lira, I. Camarillo, E. Alvarez-Ramos, A.N. Meza-Rocha, U. Caldiño, Calcium-zinc phosphate glasses activated with Tb<sup>3+</sup>/Eu<sup>3+</sup> for laser and white LED applications, J. Lumin. 215 (2019) 116621. https://doi.org/10.1016/j.jlumin.2019.116621.
- ▶ P.N. Parale, A.R. Kadam, S.J. Dhoble, K. V. Dabre, Tailored efficient energy transfer Tb<sup>3+</sup>, Eu<sup>3+</sup> activated/co-activated LiAl(PO<sub>3</sub>)<sub>4</sub> phosphor by substitution of alkali metals: the effect of charge compensation, RSC Adv. 13 (2023) 26179–26188.
- https://doi.org/10.1039/d3ra03115b.
- ➤ R.S. Yadav, Monika, E. Rai, L.P. Purohit, S.B. Rai, Realizing enhanced downconversion photoluminescence and high color purity in Dy³+ doped MgTiO₃ phosphor in presence of Li⁺ ion, J. Lumin. 217 (2020) 116810.
- https://doi.org/10.1016/j.jlumin.2019.116810.
- U. Ahmed, M.M. Shahid, S. Shahabuddin, N.A. Rahim, M. Alizadeh, A.K. Pandey, S. Sagadevan, An efficient platform based on strontium titanate nanocubes interleaved polypyrrole nanohybrid as counter electrode for dye-sensitized solar cell, J. Alloys Compd. 860 (2021) 158228. https://doi.org/10.1016/j.jallcom.2020.158228.
- A.R. Kadam, G.C. Mishra, S.J. Dhoble, Thermoluminescence study and evaluation of trapping parameters CaTiO<sub>3</sub>: RE (RE=Eu<sup>3\*</sup> Dy<sup>3\*</sup>) phosphor for TLD applications, J. Mol. Struct. 1225 (2021) 129129. https://doi.org/10.1016/j.molstruc.2020.129129.
- H. Liu, L. Mei, L. Liao, Y. Zhang, Q. Guo, T. Zhou, Y. Wang, L. Li, Strategy for realizing ratiometric optical thermometry via efficient Tb<sup>3+</sup>-Mn<sup>2+</sup> energy transfer in novel apatite-type phosphor Ca<sub>9</sub>Tb(PO<sub>4</sub>)<sub>5</sub>(SiO<sub>4</sub>)F<sub>2</sub>, J. Alloys Compd. 770 (2019) 1237−1243. https://doi.org/10.1016/j.jallcom.2018.08.167.
- ▶ J. Zhou, Z. Xia, Luminescence color tuning of Ce³⁺, Tb³⁺ and Eu³⁺ codoped and tri-doped BaY₂Si₃O₁₀ phosphors via energy transfer, J. Mater. Chem. C 3 (2015) 7552-7560. https://doi.org/10.1039/c5tc00962f.
- Z. Yahiaoui, M.A. Hassairi, M. Dammak, E. Cavalli, F. Mezzadri, Tunable luminescence and energy transfer properties in YPO<sub>4</sub>:Tb<sup>3+</sup>, Eu<sup>3+</sup>/Tb<sup>3+</sup> phosphors, J. Lumin. 194 (2018) 96–101. https://doi.org/10.1016/j.jlumin.2017.10.001.
- K. Dubey, A.R. Kadam, N. Baig, N.S. Dhoble, S.J. Dhoble, K. Dubey, A.R. Kadam, N. Baig, N.S. Dhoble, S.J. Dhoble, Wet chemically prepared terbium activated sodium calcium chlorosulfate phosphor for solid state lighting industry, Radiat. Eff. Defects Solids 2 (2020). https://doi.org/10.1080/10420150.2020.1855179.
- ▶ R. V. Tikale, A.R. Kadam, D.K. Halwar, S.J. Dhoble, Luminescence investigation of red emitting CaAlSiO<sub>4</sub>F: Eu<sup>3+</sup> doped phosphor for white LEDs based on oxyfluoride matrix, Mater. Lett. X 21 (2023) 100224. https://doi.org/10.1016/j.mlblux.2023.100224.

ISSN: 2229-7359 Vol. 11 No. 25s,2025

https://theaspd.com/index.php

➤ R. V. Tikale, A.R. Kadam, S.J. Dhoble, Optical properties and crystal structure analysis of Sr<sub>3</sub>AlO<sub>4</sub>F:Sm<sup>3+</sup>, Eu<sup>3+</sup> phosphors: an approach towards color tunability, J. Mater. Sci. Mater. Electron. 34 (2023). https://doi.org/10.1007/s10854-023-11356-z.

- A.R. Kadam, S.J. Dhoble, Energy transfer mechanism of KAlF<sub>4</sub>:Dy<sup>3+</sup>, Eu<sup>3+</sup> co-activated down-conversion phosphor as spectral converters: An approach towards improving photovoltaic efficiency by downshifting layer, J. Alloys Compd. 884 (2021) 161138. https://doi.org/10.1016/j.jallcom.2021.161138.
- A.R. Bansod, A.R. Kadam, P.S. Bokare, S.J. Dhoble, Luminescence study of Sm<sup>3+</sup>, Eu<sup>3+</sup>-doped Y<sub>2</sub>Zr<sub>2</sub>O<sub>7</sub> host: optical investigation of greenish yellow to red colour tunable pyrochlore phosphor, Luminescence (2022) 1–9. https://doi.org/10.1002/bio.4305.
- V. Bharati, S. Ramnath, Tunable emission and energy transfer of Sm<sup>3+</sup>/Eu<sup>3+</sup> activated/ co-activated Mg<sub>21</sub>Ca<sub>4</sub>Na<sub>4</sub>(PO<sub>4</sub>)<sub>18</sub> phosphors for warm light emitting diodes and display applications, J. Opt. (2024). https://doi.org/10.1007/s12596-023-01608-w.
- ➤ V. Bharati, B. Talwar, S. Meshram, Optical investigation of Dy³+/ Eu³+ co-activated K₂NaAlF₀ fluorophosphor for color tunable lighting system: Structural analysis and warm light generation, J. Mol. Struct. 1324 (2025) 140831. https://doi.org/10.1016/j.molstruc.2024.140831.
- A.R. Kadam, R.S. Yadav, G.C. Mishra, S.J. Dhoble, Effect of singly, doubly and triply ionized ions on downconversion photoluminescence in Eu<sup>3+</sup> doped Na<sub>2</sub>Sr<sub>2</sub>Al<sub>2</sub>PO<sub>4</sub>Cl<sub>9</sub> phosphor: A comparative study, Ceram. Int. 46 (2020) 3264–3274. https://doi.org/10.1016/j.ceramint.2019.10.032.
- ➤ T.S. Dhapodkar, A.R. Kadam, N. Brahme, S.J. Dhoble, Efficient white light-emitting Mg<sub>21</sub>Ca<sub>4</sub>Na<sub>4</sub>(PO<sub>4</sub>)<sub>18</sub>:Dy<sup>3+</sup>,Tb<sup>3+</sup>,Eu<sup>3+</sup> triple-doped glasses: a multipurpose glasses for WLEDs, solar cell efficiency enhancement, and smart windows applications, Mater. Today Chem. 24 (2022) 100938. https://doi.org/10.1016/j.mtchem.2022.100938.
- W. Zhang, R. Zhang, S. Yang, R. Wang, L. Na, R. Hua, Synthesis and photoluminescent features of Eu<sup>3+</sup>-doped NaGd(WO<sub>4</sub>)<sub>2</sub> nanophosphors, Mater. Res. Bull. 122 (2020) 110689. https://doi.org/10.1016/j.materresbull.2019.110689.
- J. Papan, D. Jovanović, M. Sekulić, E. Glais, M.D. Dramićanin, Photoluminescence properties and thermal stability of RE<sub>2</sub>, Eu<sub>x</sub>Sn<sub>2</sub>O<sub>7</sub> (RE = Y<sup>3+</sup>, Gd<sup>3+</sup>, Lu<sup>3+</sup>) red nanophosphors: An experimental and theoretical study, Powder Technol. 346 (2019) 150–159. https://doi.org/10.1016/j.powtec.2019.02.013.
- V. Singh, A.R. Kadam, S.J. Dhoble, H. Jeong, Luminescence studies of green emitting CaLa<sub>4</sub>Si<sub>3</sub>O<sub>13</sub>:Tb<sup>3+</sup> phosphor for WLED and PDP applications, Optik (Stuttg). 243 (2021) 167327. https://doi.org/10.1016/j.ijleo.2021.167327.
- A.R. Kadam, G.C. Mishra, A.D. Deshmukh, S.J. Dhoble, Enhancement of blue emission in Ce<sup>3+</sup>, Eu<sup>2+</sup> activated BaSiF<sub>6</sub> downconversion phosphor by energy transfer mechanism: A photochromic phosphor, J. Lumin. 229 (2021) 117676. https://doi.org/10.1016/j.jlumin.2020.117676.
- A.R. Kadam, S.B. Dhoble, G.C. Mishra, A.D. Deshmukh, S.J. Dhoble, Combustion assisted spectroscopic investigation of Dy<sup>3+</sup> activated SrYAl<sub>3</sub>O<sub>7</sub> phosphor for LED and TLD applications, J. Mol. Struct. 1233 (2021) 130150. https://doi.org/10.1016/j.molstruc.2021.130150.
- ➤ S.G.M. Mushtaque, A.R. Kadam, S.J. Dhoble, High color purity and color tunability in Sm³+/ Eu³+ activated/ co-activated Sr<sub>6</sub>Ca<sub>4</sub>(PO<sub>4</sub>)<sub>6</sub>F<sub>2</sub> phosphor for WLED and display devices application, J. Mol. Struct. 1274 (2023) 134510. https://doi.org/10.1016/j.molstruc.2022.134510.
- V. Bharati, B. Talwar, Structural and optical investigation of Tb<sup>3+</sup>/Eu<sup>3+</sup> activated/co-activated NaLa(MoO<sub>4</sub>)<sub>2</sub> phosphors by energy transfer mechanism, J. Opt. (2024). https://doi.org/10.1007/s12596-024-02173-6.
- V. Bharati, S. Ramnath, Structural investigation and red emission intensity enhancement in Sm<sup>3+</sup>/Eu<sup>3+</sup>-doped/co-doped KSrPO<sub>4</sub> phosphors: effect of charge compensation, Bull. Mater. Sci. 48 (2025). https://doi.org/10.1007/s12034-024-03350-w.